Reconstruction and structure of electrocardiogram phase portraits

P. I. Saparin,[1,2] M. A. Zaks,[1] J. Kurths,[1] A. Voss,[3] and V. S. Anishchenko[2]

[1]*Arbeitsgruppe ''Nichtlineare Dynamik'' der Max-Planck-Gesellschaft an der Universität Potsdam, Postfach 601553, D-14415 Potsdam, Germany*

[2]*Saratov State University, Saratov, Russia*

[3]*Max-Delbrueck-Centrum, Franz-Volhard-Klinik, D-13125 Buch, Germany*

The electrical activity of the heart on the short time range is studied numerically on the base of high-resolution electrocardiograms. We find that the low-amplitude part of the signal is well approximated by a superposition of two time exponents, one of them being complex. This serves as a justification to embed the whole process into a low-dimensional space. A combination of a noise reduction with time delay technique recovers a phase portrait in four-dimensional space. Its fine structure is resolved by projecting into a three-dimensional subspace, where the process resembles a nearly homoclinic motion in a system with a saddle-focus fixed point. A statistical description based on the computation of respective Shannon entropies provides a sharp distinction between healthy persons and patients with high risk for sudden cardiac death. [S1063-651X(96)10507-9]

PACS number(s): 87.10.+e, 05.45.+b

I. INTRODUCTION

The electrical activity of the heart exhibits a complex behavior on various time scales for both healthy and diseased persons. Deciphering this activity is, therefore, an important challenge to techniques of nonlinear data analysis. For the long-range interval ($\sim$24 h) a $1/f$-like power spectrum and the presence of long-range correlations in the electrocardiogram (ECG) were documented in Refs. [1–4]. The analysis of the medium range (10–60 min) started with the estimation of fractal dimension and Lyapunov exponents [5,6]; recently measures of complexity [7–9] and image processing have been used in this context. Here, we will concentrate on the short-range interval, studying the inner fine structure within the heartbeat, and aiming at the description from both the dynamical and statistical points of view. Early advances in this direction were made by Babloyantz and Destexhe, who used the direct Takens embeddings [10] for estimating the correlation dimension [5]. Another approach to evaluate the correlation dimension and the largest Lyapunov exponent was proposed in [11] where the method of singular value decomposition due to Broomhead and King [12] was utilized, and various cutoff filters were compared.

Here we suggest a different approach. Starting from high-resolution ECG data, we present the time dependence of the low-amplitude (interspike) part of the signal as a sum of several exponents. Having determined these exponents and the respective prefactors with the help of the Levenberg-Marquardt method, we observe that the signal can be reasonably well represented by the superposition of only two exponents, one of these being complex. Keeping this in mind, we further combine the noise reduction technique suggested by Schreiber and Grassberger [13,14] with the time-delay reconstruction in a four-dimensional space; to enhance the resolution of the fine structure, we project the obtained attracting object with a special technique [15] into a three-dimensional subspace. This processing of the data is described in Sec. II; Sec. III provides the dynamical interpretation of the motion

in the reconstructed phase space, which proves to be similar to the motion in a system with a saddle-focus fixed point close to homoclinicity. A statistical description based on the computation of Shannon entropies for two-dimensional distributions is presented in Sec. IV.

The reconstructed phase portraits display a qualitative difference (geometry of the attractor, number of fixed points) between healthy persons and those with a high risk for sudden cardiac death. This circumstance points to the possibility of the application of the proposed technique to improve the diagnostics of this disease.

II. DATA PROCESSING AND PHASE SPACE RECONSTRUCTION

For our analysis we have used high-resolution ECG data recorded from six healthy persons and seven patients with a high risk of sudden cardiac death. Each dataset is a 3-min record with the sampling frequency 2 kHz and 16-bit resolution under the condition of rest. Of the three Frank electrocardiographic leads [16] we have chosen that one with the most pronounced patterns of the signal, i.e., the P, QRS, and T waves (Fig. 1).

Traditionally in vectorcardiography one uses simultaneous values of signals from three leads, which sample the data from the electrodes lying in three orthogonal planes. The amplitude and the direction of the resulting time-dependent vector reflect the integral spatiotemporal evolution of the electrical field in the heart. The set of vectors obtained during one cardiac cycle forms the vectorcardiogram. In terms of phase space dynamics this procedure recovers the projection of the respective phase portrait into the three-dimensional subspace. It is important to note that in this subspace the planes in which the loops corresponding to P, QRS, and T waves lie, are distinctly not parallel. The embedding technique enables the reconstruction of phase portraits from time series delivered by a single lead [10]. We will start our reconstruction from the closer view at the
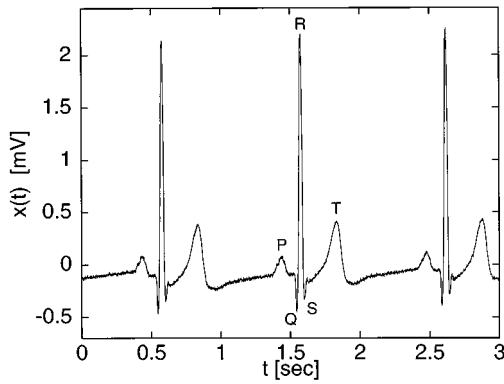
FIG. 1. Raw ECG data with sampling rate 2 kHz from a healthy person. The outstanding extrema are termed in cardiology P wave, QRS complex, and T wave.

"calm" segments of the ECG.

As can be seen from the shape of the ECG, the "active" segments with pronounced variation are relatively short, and most of the beat duration is spent in a slow low-amplitude motion, i.e., in the P-Q, S-T, and T-P intervals. Due to their low voltage these segments at which the pen or the electron beam simply returns back to zero, are usually nonresolvable for the traditional vectrocardiography. The precision of the data employed here allows us to concentrate on these intervals; assuming that at this stage the evolution is linear (plus noise), we can estimate the amount of the contributing normal modes as well as the characteristic times of the respective (possibly complex) exponents. The latter are associated to the growth and decay rates of the electric disturbances in the heart tissues. Thus we take one of the low-amplitude segments, which usually contains about 100 points, and assume that the signal $U(t)$ can be represented as a sum $U(t) = U_0 + \Sigma_{i=1}^{N} U_n \exp(\gamma_n t)$. The unknown parameters U_n and γ_n have been found by fitting the data with the help of the Levenberg-Marquardt method. An approximation with $N = 5$ provides quite satisfactory results. For every person the variation of exponent values for different low-amplitude parts within a single heartbeat is insignificant; from one beat to another it is moderate ($\leqslant 20\%$), which can be attributed to the weak influence exerted on the tissue characteristics by the middle-range effects such as respiration. For the record, from Fig. 1 we obtained $\gamma_1 = 145$, $\gamma_{2,3} = -86 \pm 141i$, $\gamma_4 = -427$, and $\gamma_5 = -1454$ (all values are expressed in sec^{-1}).

Within the group of healthy persons the variations of the exponents are moderate. The qualitative picture persists: the signal can be decomposed into the decaying oscillations and three monotonic terms; the latter are characterized by the exponents, one of which is positive and the other two negative and relatively large in the absolute value. The positive exponent should not be necessarily interpreted as an indication of the permanent presence of some unstable mode in the process. The value of the respective prefactor is small (compare $U_1 = 1.3 \times 10^{-3}$, $|U_2| = 7.67$), which means that for a good part of the interval the growing mode is hardly distinguishable at the background of the decaying process; its rapidly growing contribution becomes noticeable (and very soon overwhelming) only after the activation of the respective part of the heart (atria or ventricles).

The decay rates γ_4 and γ_5 are rather large as compared to $\mathrm{Re}(\gamma_{2,3})$. Correspondingly the contribution of the respective modes into the whole signal is almost negligible. With reasonable accuracy one may, hence, embed the low-amplitude part of the beat proceeds into the subspace spanned by three modes corresponding to γ_1 and $\gamma_{2,3}$. Thus, one is tempted to undertake the attempt of the reconstruction of the whole phase portrait (including the spikes) in a low-dimensional space, possibly even three dimensional. Although some of the fine differential details may get lost, we can hope that essential basic features of the portrait can be captured already by this truncation. The obvious criterion in this case should be the absence of the self-intersections of trajectories.

Before proceeding to the reconstruction itself we reduce the noise level. As a first step we apply the low-pass Butterworth filters of the sixth order [17] with the cutoff frequency 43 Hz, thus getting rid of the possible external periodic influences such as the pollution with the ac frequency (50 Hz). In our further filtering we do not use the method of singular value decomposition suggested by Broomhead and King [12], since its application, although qualitatively preserving the topology, may result in severe changes of the relative amplitudes of the ECG wave components. Instead we utilize the nonlinear noise reduction algorithm of Schreiber and Grassberger [13]. Here follows a sketch of this method as applied to our task. The scalar time series is embedded into the seven-dimensional (this number proved to be computationally optimal) space composed by the delay and advanced coordinates: $\vec{u}_n = (u_{n-3}, u_{n-2}, u_{n-1}, u_n, u_{n+1}, u_{n+2}, u_{n+3})$. For each vector $\vec{u}_n$ all neighbors localized in a small neighborhood of radius $\delta = 0.01$ are detected. Then u_n is replaced by $\hat{u}_n$ obtained by local averaging. This procedure is iterated $4-7$ times until the value of correction $\|\hat{\hat{u}}_n - \vec{u}_n\|$ is less than $\varepsilon = 5.0 \times 10^{-7}$. The final output is a new scalar series in which the high-frequency components and the external influence are suppressed, and the noise is strongly reduced, but the shape of the ECG curve and the relative amplitudes of its wavetrains are retained.

Here we would like to note that one may first perform the noise reduction and only then expand the low-amplitude part of the obtained filtered signal into the real and complex time exponents, as described above. Our results have confirmed that the numerical values characterizing the decay and growth times almost do not depend on the order of these operations.

As a next step, the data are embedded into a four-dimensional space using the delay coordinates, and further projected into the three-dimensional space with the use of a special technique described in [15]. The particularities for our case are relegated to the Appendix. Varying the projection vector, we obtain different three-dimensional (3D) pictures and examine the phase portrait from different directions. Generically, the structure of the reconstructed object does not depend on the projection (naturally, with the condition that there are no orbit self-intersections). On the other hand, it is possible to attain a better graphical resolution for the domains of special interest, which for us is the central part of the reconstructed object. The coordinates of the projection vector that we found to be the most appropriate one were fixed in all the further experiments.

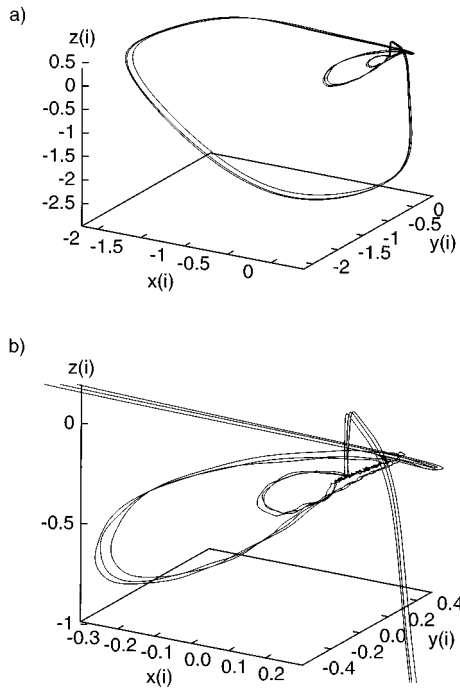Although the topology of the phase portraits for the same

FIG. 2. Phase portrait reconstruction by direct Takens embedding into three-dimensional space, obtained from a single ECG lead of a healthy person. Global view (a) and central part (b).

three cardiac cycles obtained either by the three-dimensional Takens embedding (Fig. 2) or by the four-dimensional embedding with subsequent projection into three-dimensional space (Fig. 3) is surely the same, the latter method allows one to resolve many more of the subtle details. This differ-
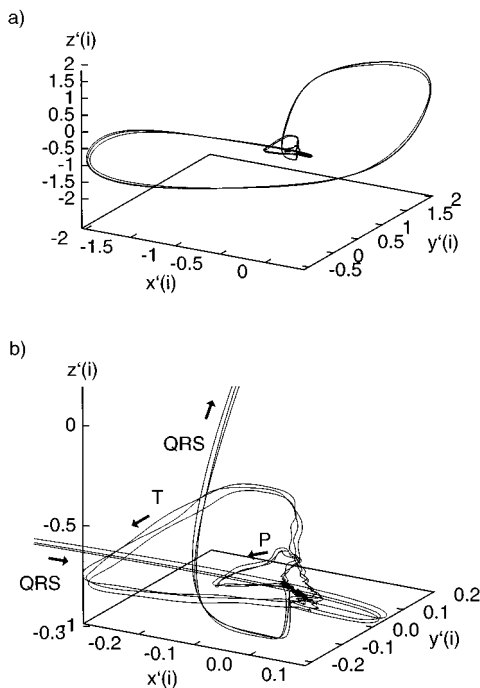

FIG. 3. Parallel projection into a three-dimensional subspace of the phase portrait obtained by embedding into a four-dimensional space for the same data as in Fig. 2. Global view (a) and the central part (b).
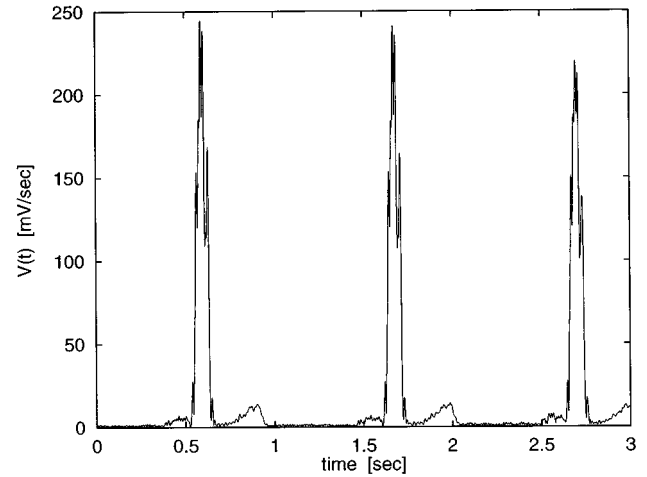

FIG. 4. Velocity of the imaging point in the reconstructed four-dimensional space for the ECG from Fig. 1.

ence is especially visible for the segments of condensation of imaging points corresponding to the P-Q, S-T, and T-P intervals of the ECG. The object reconstructed from direct three-dimensional embedding has a rather ''planar'' shape, which is also confirmed by the investigation of its transversal Poincaré section. In this sense the four-dimensional embedding with its angles between the planes of different loops is closer to the real vectrocardiogram constructed on the base of three orthogonal leads. As a consequence the mentioned intervals are now clearly structured and allow for the further measurements.

III. GEOMETRY OF RECONSTRUCTED ORBITS

Let us have a closer look at the details of the phase space representation (Fig. 3). Now the low-amplitude part of the ECG, where the imaging point spends a noticeable part of the time (aforementioned segments P-Q, S-T, and T-P), corresponds to the vicinity of the origin of the reconstructed space. The trajectory departs from this region to form three outstanding loops: the largest, the medium, and the minor ones correspond to the QRS complex, T wave, and P wave, respectively. As seen from Fig. 3(b), the imaging point departs from the central region either upwards (P and T loops) or downwards (QRS complex) and then returns back to it. The returning segment of the orbit is an almost planar spiral that is winding onto the origin.

In summary, the data recover the plane along which the trajectories are returning to the origin and two directions of the escape; this looks very much like a motion near the fixed point of the saddle-focus type [18] with the locally planar two-dimensional stable manifold and the one-dimensional unstable manifold. The escaping trajectories depart along either of the two components of the latter until some global reinjecting force makes them return to the fixed point and perform several revolutions around it. Thus, the assumption that the observed system is close to the dynamical system with the homoclinic connection to the saddle focus looks quite plausible. It is further corroborated by the temporal distribution of the orbital velocity defined in terms of the embedding coordinates: as can be seen from Fig. 4, the process is composed of long segments of relatively slow motion

interspersed by short violent bursts. The velocity is maximal in the central part of the loop; on the contrary, it almost vanishes near the origin.

According to Shil'nikov [19], the dynamics for systems close to those with a homoclinic orbit to the saddle focus is entirely determined by the eigenvalues $\sigma \pm i\omega$ and λ ($\sigma < 0 < \lambda$) of the linearization of the vector field near the fixed point. In our case σ is the damping of the spiral coils, ω is the rotation frequency in the spiral, and λ gives the rate of escape from this singular point. Naturally, these eigenvalues are nothing else but the exponents γ_i evaluated above with the help of numerical fitting: $\lambda = \gamma_1$, $\sigma = \text{Re}(\gamma_2)$, $\omega = \text{Im}(\gamma_2)$. According to the numerical estimates, $\gamma > |\sigma|$, which would mean that at the moment of the formation of the homoclinic loop the system possesses an infinite number of horseshoes and, consequently, countably many unstable periodic orbits. It should be noted that the corresponding chaotic set need not necessarily be attracting. Being apparently close to homoclinicity, our reconstructed dynamical system seems to retain the chaotic features: although the rough outlines are reproduced with each new heartbeat, the finer details may vary. One may roughly consider the whole beat as a sequence of different wavetrains; although the ordering of the waves is prescribed, their amplitudes vary slightly from beat to beat, which corresponds to different positions within a band of a multibanded attractor.

The first reconstruction of a Poincaré section from the ECG data was described in [5]. We have computed Poincaré mappings for different planes in the reconstructed phase space; for this purpose the advantage of the initial four-dimensional embedding is that it eliminates the strong global stretching, which is typical for the direct 3D embedding. The shape of the mapping depends on the location of the plane: there is a horseshoe-shaped stripe induced by the points from the P interval and a spurge for the points from the region R. This reflects the complicated stretching and folding that is exerted upon the bundle of neighboring trajectories in different regions of the phase space.

Figures 5(a) and 5(b) present the phase portraits reconstructed by four-dimensional embedding from 200 heart cycles of healthy and diseased humans, respectively. The differences in geometry (form of the branches, directions of escape, etc.) can be clearly seen. In some pathological cases instead of a single fixed point (typical for a healthy person) one detects two fixed points; after hovering over one of them, the system does not proceed to the next loop but instead passes to the second fixed point and spends a noticeable time there. This raises the question of whether the portrait of a normal state of the cardiovascular system differs from the diseased one by the number of fixed points and/or the possibilities to visit their localities. Thus the central region of the ECG and the local properties of the flow near the conjectural fixed point seem to play an important role in the distinction between the healthy person and the cardiac patient.

IV. STATISTICAL DESCRIPTION

As explained above, the behavior in the central region seems to be especially important in distinguishing between healthy and diseased states. There are two different ways to
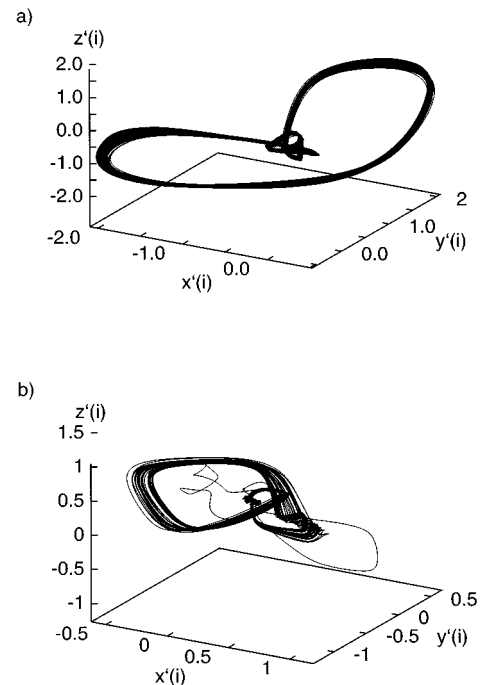

FIG. 5. Phase portraits for ~ 200 heart beats obtained by parallel projection from 4D into 3D. (a) Healthy person; (b) person with a high risk for sudden cardiac death.

separate this region of interest from the entire ECG attractor. As we have established numerically the kinematic partition, where the region corresponding to the lowest phase velocity is singled out, provides better results than the purely geometrical choice of a particular spatial domain. As the optimum value for the level of velocity defining the central region, our experiments give the value of 5 mV/sec, which approximately corresponds to the maximal velocity of the phase point during the P loop. We should note that the reasonable variations of this limit do not sensitively influence the results.

Our statistical procedure to analyze the central domain of the attractor consists of the following steps:

(1) Garner the intervals of trajectories on which the velocity of the phase point in the reconstructed space is less than a given level.

(2) To quantify statistically the structure and complexity of this region, (a) we project the reconstructed object onto the horizontal plane and estimate the two-dimensional distribution of the residence time using the partition of this plane into $m \times n$ cells (Fig. 6). (b) Already a graphical representation displays a nonambiguous difference between a well-structured distribution stemming from the healthy person and the fuzzy landscape derived from the ill patient. To provide the quantitative characterization of this difference, we calculate the Shannon entropy of this distribution

$$S = -\sum_{i=1}^{m}\sum_{j=1}^{n} p_{ij}\ln(p_{ij}), \quad \sum_{i=1}^{m}\sum_{j=1}^{n} p_{ij} = 1,$$

(3) Having computed the mean value $\langle S \rangle$ of S for all healthy persons we relate the individual value for each patient
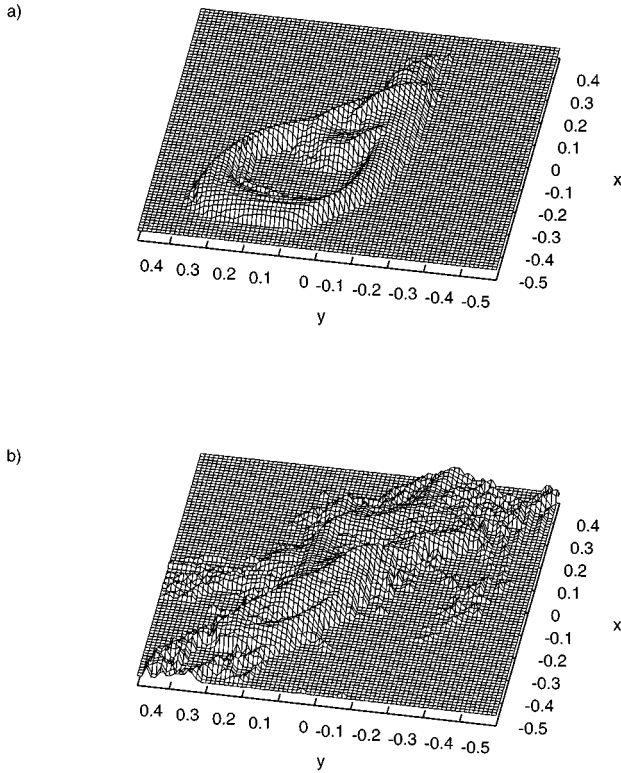
a)

b)

FIG. 6. Distribution of residence times for the projection of the imaging point onto the x'-y' plane of the reconstructed space. The upper limit of velocity is 20 mV/sec. The scale in vertical direction is logarithmic. (a) Healthy person; (b) person with a high risk for sudden cardiac death.
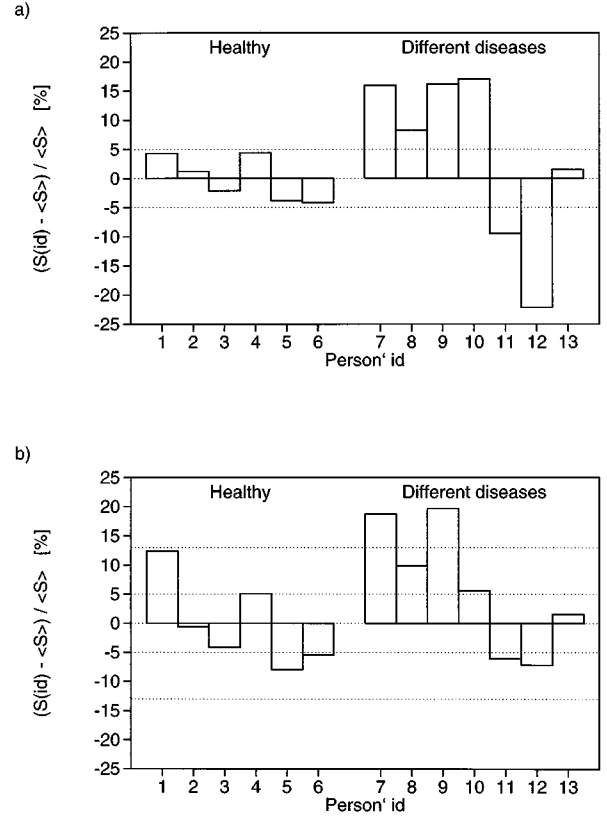
a)

b)

FIG. 7. Shannon entropies of 2D distributions, related to the average value $\langle S \rangle$. (a) Estimate based on projection from four-dimensional space; (b) estimate based on direct three-dimensional embedding.

$S(id)$ to this averaged quantity. We have established that increase of m and n beyond 40 does not influence this normalized value; the distributions in Fig. 6 correspond to $m = n = 80$.

As a result of investigation of six healthy persons and seven ill patients with a high risk for sudden cardiac death we get a surprisingly good distinction between these two groups [Fig. 7(a)]. The entropies of all the healthy persons fall within a narrow range of $\pm 5\%$ from the mean value $\langle S \rangle$ while the values for six ill patients lie outside this range. Only one ill person is not recognized in this way. In order to compare our technique with conventional methods, we applied the procedure described above to the data embedded directly into the three-dimensional space. Notably, this straightforward embedding fails to provide such a sharp distinction [cf. Fig. 7(b)].

V. CONCLUSIONS

We have applied dynamical and statistical analysis to several ECG's of healthy persons and patients with a high risk for sudden cardiac death. It proved to be possible to reconstruct the structure of the heart electrical activity from a single ECG lead. Compared to the traditional vectorcardiography this approach does not demand an additional correction of the obtained signals due to nonorthogonality of the leads. The embedding-projection technique [15] resolves the

structure of the underlying attractor better than the direct Takens embedding.

In order to distinguish between healthy and diseased persons, the calculation of two-dimensional Shannon entropy from the central region (defined through the low velocity values) seems to be very promising: most of the patients with high risk have been recognized in this way.

Finally, we would like to emphasize that these preliminary results have to be checked against a larger and more representative data set stemming from a large number of persons.

APPENDIX: EMBEDDING AND PROJECTING

A special technique for investigating objects in four-dimensional space has been described in [15]. With respect to our ECG data the procedure is the following.

At first the data $u(t)$, $t = i\Delta_t$, $i = 0, \ldots, N-1$ are embedded into four-dimensional space $[x,y,z,w]$ using the delay coordinates $x(t) = u(t)$, $y(t) = u(t+\tau)$, $z(t) = u(t+2\tau)$, $w(t)$

$= u(t+3\tau)$, $\tau = l\Delta_t$. In our experiment $\Delta_t = 0.0005$ sec; the optimal l (for which the P, T, and QRS loops are neither too compressed nor too stretched) has been found to be $l = 26$, consequently, $\tau = 0.013$ sec.

To analyze the geometry and structure of the obtained four-dimensional object we take a parallel projection into a three-dimensional space $[x', y', z']$:

$$x'(t) = p_2 x(t)/A - p_1 y(t)/A,$$

$$y'(t) = p_1 p_3 x(t)/AB + p_2 p_3 y(t)/AB - Az(t)/B,$$

$$z'(t) = p_1 p_4 x(t)/B + p_2 p_4 y(t)/B + p_3 p_4 z(t)/B - Bw(t),$$

where $\vec{p}$ is a unit projection vector

$$\vec{p} = (p_1, p_2, p_3, p_4), \quad \|\vec{p}\| = 1 \quad \text{and} \quad A = \sqrt{p_1^2 + p_2^2},$$

$$B = \sqrt{p_1^2 + p_2^2 + p_3^2}.$$

By changing $\vec{p}$ one gets different projections into the three-dimensional space and views the phase portrait from different directions. From the point of view of the orbit geometry, as well as for the projection onto the two-dimensional plane with subsequent statistical analysis, the central part of the reconstructed object is of special interest. We have found that its structure is best resolved with the values $p_1 = 0.1$, $p_2 = 0.75$, and $p_3 = 0.153$.

---

[1] M. Kobayashi and T. Musha, IEEE Trans. Biomed. Eng. **29**, 456 (1982).

[2] A. L. Goldberger, New in Physiol. Sci. **6**, 87 (1991).

[3] C.-K. Peng, J. Mietus, J. M. Hausdorff, S. Havlin, H. E. Stanley, and A. L. Goldberger, Phys. Rev. Lett. **70**, 1343 (1993).

[4] L. Glass and M. C. Mackey, *From Clocks to Chaos: The Rhythms of Life* (Princeton Univ. Press, Princeton, 1988).

[5] A. Babloyantz and A. Destexhe, Biol. Cybern. **58**, 203 (1988).

[6] G. Mayer-Kress, F. E. Yates, F. Benton, M. Kiedel, W. Tirsch, S. J. Pöppel, and K. Geist, Math. Biosci. **90**, 155 (1988).

[7] J. Kurths, A. Voss, P. Saparin, A. Witt, H. J. Kleiner, and N. Wessel, Chaos **5**, 88 (1995).

[8] J. J. Żebrowsky, W. Poplawska, and R. Baranowski, Phys. Rev. E **50**, 4187 (1994).

[9] A. Voss, J. Kurths, N. Wessel, A. Witt, P. Saparin, and R. Dietz, Cardiovascular Res. J. European Soc. Cardiol. **31**, 419 (1996).

[10] F. Takens, *Detecting of Strange Attractors in Turbulence*, Lecture Notes in Mathematics Vol. 898 (Springer, Berlin, 1981),

pp. 366–381.

[11] V. Anishchenko, P. Saparin, and M. Safonova, Radiotech. Elektron. **37**, 467 (1992).

[12] D. S. Broomhead and G. P. King, Physica D **20**, 217 (1986).

[13] T. Schreiber and P. Grassberger, Phys. Lett. A **160**, 411 (1991).

[14] T. Schreiber, Phys. Rev. E **47**, 2401 (1993).

[15] K. Miyazaki and K. Ishihara (unpublished); I. Tsuda, T. Tahra, and H. Iwanaga, Int. J. Bifur. Chaos **2**, 313 (1992).

[16] H. Friedman, *Diagnostic Electrocardiography and Vectorcardiography* (McGraw-Hill, New York, 1971); A. Bayes de Luna, *Textbook of Clinical Electrocardiography* (Martinus Nijhoff Publishers, Dordrecht, 1987).

[17] D. F. Elliot, *Handbook of Digital Signal Processing* (Academic, San Diego, 1987).

[18] J. Guckenheimer and P. Holmes, *Nonlinear Oscillations, Dynamical Systems, and Bifurcations of Vector Fields* (Springer, New York, 1983).

[19] L. P. Shil'nikov, Math. Sbornik **81**, 92 (1970).